



Hormone-sensitive lipase protects adipose triglyceride lipase-deficient mice from lethal lipotoxic cardiomyopathy

Mika Yamada¹, Jinya Suzuki^{1,2*}, Satsuki Sato¹, Yasuo Zenimaru¹, Rie Saito¹, Tadashi Konoshita¹, Fredric B. Kraemer^{3,4}, and Tamotsu Ishizuka¹

¹Third Department of Internal Medicine, Faculty of Medical Sciences, University of Fukui, Fukui, Japan; ²Department of Medicine, Medical Corporation Yasukawa Hospital, Fukui, Japan; ³Division of Endocrinology, VA Palo Alto Health Care System, Palo Alto, CA, USA; ⁴Division of Endocrinology, Stanford University, Stanford, CA, USA

Abstract Lipid droplets (LDs) are multifunctional organelles that regulate energy storage and cellular homeostasis. The first step of triacylglycerol hydrolysis in LDs is catalyzed by adipose triglyceride lipase (ATGL), deficiency of which results in lethal cardiac steatosis. Although hormone-sensitive lipase (HSL) functions as a diacylglycerol lipase in the heart, we hypothesized that activation of HSL might compensate for ATGL deficiency. To test this hypothesis, we crossed ATGL-KO (AKO) mice and cardiac-specific HSL-overexpressing mice (cHSL) to establish homozygous AKO mice and AKO mice with cardiac-specific HSL overexpression (AKO+cHSL). We found that cardiac triacylglycerol content was 160-fold higher in AKO relative to Wt mice, whereas that of AKO+cHSL mice was comparable to the latter. In addition, AKO cardiac tissues exhibited reduced mRNA expression of PPAR α -regulated genes and upregulation of genes involved in inflammation, fibrosis, and cardiac stress. In contrast, AKO+cHSL cardiac tissues exhibited expression levels similar to those observed in Wt mice. AKO cardiac tissues also exhibited macrophage infiltration, apoptosis, interstitial fibrosis, impaired systolic function, and marked increases in ceramide and diacylglycerol contents, whereas no such pathological alterations were observed in AKO+cHSL tissues. Furthermore, electron microscopy revealed considerable LDs, damaged mitochondria, and disrupted intercalated discs in AKO cardiomyocytes, none of which were noted in AKO+cHSL cardiomyocytes. Importantly, the life span of AKO+cHSL mice was comparable to that of Wt mice. **HSL overexpression normalizes lipotoxic cardiomyopathy in AKO mice and the findings highlight the applicability of cardiac HSL activation as a therapeutic strategy for ATGL deficiency-associated lipotoxic cardiomyopathies.**

Supplementary key words apoptosis • beta-oxidation • ceramides • FA • lipid droplets • lipotoxicity • macrophage • mitochondria • perilipins • triacylglycerol

Lipid droplets (LDs) are intracellular organelles found in various cell types within the body. In cardiomyocytes, long-chain FAs, which are considered the major dietary FAs utilized by cardiac tissue, are subjected to uptake via FA transporters, following which they are converted to acyl-CoAs and directly oxidized or converted to triacylglycerol (TAG) for storage in LDs (1).

LD synthesis and degradation are dynamically regulated in the heart depending on the cardiac energy status. Under conditions with increased plasma FA levels, for example, diabetes or obesity, the FA influx often exceeds the cellular capacity for FA oxidation (FAO), resulting in intracellular LD accumulation (steatosis) (2, 3). Aberrant LD accumulation, associated with stimulated intracellular lipolysis, is thought to induce intracellular lipotoxicity. FAs released from LDs stimulate ceramide biosynthesis and lipid peroxidation, which in turn induce apoptosis (4, 5). Excess FAs also increase intracellular fatty acyl-CoAs and diacylglycerol (DAG) levels, triggering the occurrence of endoplasmic reticulum (ER) stress and insulin resistance (6, 7). These adverse reactions lead to cardiac dysfunction, namely lipotoxic cardiomyopathy (8).

Cardiac steatosis is also present in conditions with impaired FAO. Genetic defects of the genes regulating FAO, such as *SLC22A5* (encoding organic cation/carnitine transporter type 2) (9, 10) or *CPT2* (encoding carnitine palmitoyltransferase 2), lead to the development of cardiac dysfunction associated with myocardial lipid accumulation (11, 12). Among mouse models, cardiac-specific PPAR δ -KO mice or heterozygous *CPT1*-KO mice reportedly develop lipotoxic cardiomyopathy with cardiomyocyte apoptosis and interstitial fibrosis (13, 14). Under such conditions, impaired FAO is considered the primary cause of cardiac dysfunction, although pathophysiological function of accumulated LDs remains to be addressed.

The TAG stored in LDs is hydrolyzed upon demand, resulting in the release of FAs for ATP production. The first step of this lipolytic cascade is catalyzed by adipose

*For correspondence: Jinya Suzuki, jinya@u-fukui.ac.jp.

triglyceride lipase (ATGL). One molecule of FA is released from the first step of the cascade to generate DAG, which is then hydrolyzed by hormone-sensitive lipase (HSL) to release FA and monoacylglycerol (MAG). In the final step, MAG is hydrolyzed by MAG lipase to release FA and glycerol (15, 16). It has been shown that intracellular TAG hydrolysis by ATGL plays a critical role in the release of essential mediator(s) involved in the generation of PPAR α lipid ligands and, consequently, modulates mitochondrial biogenesis as well as oxidative phosphorylation (17). Thus, ATGL plays an important role not only in controlling intracellular energy supply but also in the regulation of cardiac gene expression and mitochondrial function.

Mutations in *PNPLA2* (which encodes ATGL) cause neutral lipid storage disease with myopathy (NLSDM). NLSDM is characterized by the presence of TAG-containing LDs in the cytoplasm of neutrophils (Jordans' bodies) as well as in the cells of other tissues, including muscle, liver, and heart tissues (18). Patients with NLSDM are primarily affected by progressive myopathy, cardiomyopathy, coronary atherosclerosis, diabetes, hepatomegaly, chronic pancreatitis, and short stature. Progressive skeletal muscle myopathy is always present, exhibiting both proximal and distal distribution (19, 20). Cardiac dysfunction is present in approximately 40–50% of patients with NLSDM, with cardiomyopathy demonstrating lethality or necessitating the conduction of cardiac transplantation in certain cases (18, 19, 21).

ATGL-KO mice were previously established as a murine model of NLSDM. They present with accumulation of massive LDs in cardiomyocytes and succumb before 6 months of age because of heart failure (22). Defective intracellular FA release from LDs and resultant mitochondrial dysfunction are considered the primary causes of cardiomyopathy in ATGL-KO mice, although the precise mechanisms through which ATGL deficiency induces such severe lipotoxicity remain to be fully understood.

PPAR α agonists reportedly normalize the expression of PPAR α -regulated genes, restore normal cardiac function, and prevent premature death in ATGL-KO mice (17). Two patients with NLSDM were previously treated with PPAR α agonist bezafibrate for a period of 28 weeks, and this led to improved FAO and reduced tissue TAG accumulation without considerable improvement in clinical parameters (23). Recently, medium-chain FA tricaprins was shown to improve myocardial long-chain FA metabolism, cardiac steatosis, and left ventricular (LV) function in ATGL-KO mice (24), incentivizing a clinical trial in Japan, which is currently ongoing. Nevertheless, an effective therapeutic strategy has not been introduced, and many ATGL-deficient patients develop heart failure at a young age, while awaiting cardiac transplantation (18, 21).

In the physiological setting, HSL functions as a DAG lipase within the heart (25), while also exhibiting potent

TAG hydrolase activity (26). We have previously reported that cardiac overexpression of HSL inhibits myocardial steatosis and fibrosis in mice with streptozotocin-induced diabetes (27) as well as atrial steatosis and atrial fibrillation in cardiac perilipin (PLIN) 2-overexpressing mice (28, 29). In the present study, we investigated whether the activation of cardiac HSL could alleviate cardiomyopathy in ATGL-KO mice. Our findings highlight the potential applicability of HSL as a therapeutic target against ATGL deficiency-associated cardiac death.

MATERIALS AND METHODS

Animal studies

Heterozygous ATGL-KO mice on a C57BL/6 background were purchased from The Jackson Laboratory (Bar Harbor, ME) (22). Cardiac-specific HSL-overexpressing mice were generated using myosin heavy chain α promoter and rat HSL complementary DNA as per methods previously reported (27) and were backcrossed to C57BL/6 mice for 10 generations. The heterozygous ATGL-KO and cardiac HSL-overexpressing mice were crossed to generate breeders of experimental groups: (ATGL^{+/-}, HSL^{Tg⁻/Tg⁻}) and (ATGL^{+/-}, HSL^{Tg⁺/Tg⁻}) mice. The breeder mice were then crossed to generate the experimental groups: Wt (ATGL^{+/+}, HSL^{Tg⁻/Tg⁻}; designated as Wt), homozygous ATGL-KO (ATGL^{-/-}, HSL^{Tg⁻/Tg⁻}; designated as AKO), heterozygous cardiac-specific HSL overexpression (ATGL^{+/+}, HSL^{Tg⁺/Tg⁻}; designated as cHSL), and AKO with cardiac-specific HSL overexpression (ATGL^{-/-}, HSL^{Tg⁺/Tg⁻}; designated as AKO+cHSL) mice. Mice from all groups were provided a regular chow diet (MF, Oriental Yeast Co, Tokyo, Japan) and water ad libitum, while kept under a 12:12 h dark-light cycle. Mice were anesthetized with isoflurane at the age of 10–12 weeks and dissected between 10:00 and 12:00 PM. All procedures were conducted in accordance with the “Regulations for Animal Research” at the University of Fukui and approved by the Animal Research Committee, University of Fukui (approval no.: R01028).

Blood chemistry

Blood samples were collected from the right ventricle under anesthesia. Plasma concentrations of FFA, TAG, and total cholesterol (T-Cho) were measured using commercially available kits (Wako, Osaka, Japan). The plasma glucose (PG) concentration was measured using Freestyle™ (Nipro, Osaka, Japan).

Western blot analysis

Immunoblot analyses were performed using specific antibodies against ATGL (catalog no.: 2439; Cell Signaling Technology, Danvers, MA), HSL (catalog no.: 4107; Cell Signaling Technology), PLIN1 (catalog no.: ab172907; Abcam, Cambridge, UK), PLIN2 (catalog no.: ab52356; Abcam), PLIN3 (catalog no.: ABS482; Merck Millipore, Burlington, MA), PLIN4 (catalog no.: 55404-1-AP; Proteintech, Rosemont, IL), PLIN5 (catalog no.: PAB12542; Abnova, Taipei, Taiwan), GAPDH (catalog no.: MAB374; Merck Millipore), phosphorylated HSL Ser563 (catalog no.: 4139; Cell Signaling Technology), Ser565 (catalog no.: 4137; Cell Signaling Technology),

Ser660 (catalog no.: 4126; Cell Signaling Technology), and phosphorylated PLIN1 (catalog no.: 3834; Affinity Biosciences, Cincinnati, OH) as per methods previously reported (29). Cardiac tissues were homogenized in TES buffer (20 mM Tris, 1 mM EDTA, 255 mM sucrose, pH 7.4) containing a protease inhibitor cocktail (catalog no.: 25955; Nacalai Tesque, Kyoto, Japan), and the supernatant was collected to be utilized in the subsequent gel electrophoresis. To analyze phosphorylated proteins, cardiac tissues were homogenized in the same TES buffer containing a phosphatase inhibitor cocktail (catalog no.: 07574; Nacalai Tesque). Next, 10–20 µg of the protein samples were subjected to SDS-PAGE, transferred to nitrocellulose membranes, and probed with the specific antibodies. The membranes were washed and incubated with the appropriate HRP-conjugated secondary antibodies (catalog no.: NA934 or no. NA931; Cytiva, Marlborough, MA), followed by chemiluminescence detection using ECL™ Prime Western Blotting Detection Reagents (catalog no.: RPN2232; GE Healthcare, Chicago, IL) and FUSION SOLO S (Vilber-Lourmat, Collégien, France). Band intensities were quantified using the Evolution-Capt Edge software, version 18.07 (Vilber-Lourmat), and protein abundance was presented relative to GAPDH in the corresponding lane.

TAG hydrolase activity assay

TAG hydrolase activity was assessed using a commercially available kit (catalog no.: MAK046; Sigma-Aldrich, St. Louis, MO), which contains the TAG substrate, following the manufacturer's protocol with a minor modification. Cardiac tissues were homogenized in TES buffer containing a protease inhibitor cocktail (catalog no.: 25955; Nacalai Tesque), and the supernatants were used for the assays. Next, 50 µl of the sample was incubated with 100 µl of the reaction mix or the sample blank mix at 37°C for 60 min. Absorbance at 570 nm was measured using a SpectraMax™ iD3 microplate reader (Molecular Devices, San Jose, CA), and the TAG hydrolase activity was calculated and presented as nanomole glycerol/minute/gram protein.

Tissue lipid content

The heart was perfused with 3 ml of PBS from the LV and was subsequently excised. Tissue samples (30–40 mg) were homogenized in 20 volumes of PBS, and lipids were extracted with 20 volumes of chloroform/methanol (2:1). After centrifugation, the chloroform phase was transferred into glass tubes, following which it was dried and dissolved in isopropyl alcohol at 70°C for 1 h. TAG level was measured using assay kits (Wako) with lipid standards that were treated in parallel with tissue samples derived from the extraction step (28).

Histological studies

The excised LV was fixed with 4% paraformaldehyde-PBS for 1 h and embedded in OCT compound (Sakura Finetek, Tokyo, Japan). The sections were stained with hematoxylin and eosin or specific antibodies against N-cadherin (catalog no.: ab98952; Abcam) for intercalated discs (ICDs) or F4/80 (catalog no.: 14-4801-85; Invitrogen, Waltham, MA) for macrophages, followed by microscopic examination using AX80 (Olympus, Tokyo, Japan). Fibrosis was assessed using Masson's trichrome staining. For confocal microscopy, the sections were stained with specific antibodies against PLIN2 or F4/80 and fluorescent secondary antibodies (catalog no.: A32733; Thermo Fisher Scientific, Waltham, MA, or catalog no.:

ab150165; Abcam, respectively), followed by observation using a confocal microscope system TCS Sp2 (Leica, Wetzlar, Germany) (29). Apoptosis was analyzed via TUNEL assay using a commercially available kit (catalog no.: MK500; Takara, Shiga, Japan).

Electron microscopy was performed as per methods previously described (29). Briefly, mouse hearts were excised and fixed with 2% paraformaldehyde and 2% glutaraldehyde in 0.1 M phosphate buffer (pH 7.4), followed by incubation in 1% osmium tetroxide for 2 h at 4°C. The samples were subjected to washing steps with 10% sucrose, stained with 2% uranyl acetate for 60 min at 4°C, dehydrated with ethanol, and embedded in epoxy resin (Quetol 812; Nisshin EM, Tokyo, Japan). Thin sections (60–70 nm in thickness) were stained with lead citrate and uranyl acetate prior to examination under a transmission electron microscope (H-7650; Hitachi, Tokyo, Japan).

Ultrasonography

Cardiac function was evaluated via echocardiography in mice that were awake, using an ultrasonograph equipped with a 13-MHz linear transducer (Aloka, Tokyo, Japan), as per protocols previously described (30).

Quantitative RT-PCR

Total RNA extraction from cardiac ventricles was performed using the Trizol™ reagent (Invitrogen), and 2 µg of RNA samples were reverse-transcribed using a Quantitect™ reverse transcription kit (Qiagen, Hilden, Germany). The reverse-transcribed samples were diluted 10 times (or two times for PLIN1) with 10 mM Tris, 1 mM EDTA, pH 8.0 buffer. The target gene transcripts were amplified and analyzed in triplicate using TaqMan™ probes (Applied Biosystems, Waltham, MA) and StepOne Software, version 2.1 (Applied Biosystems) as previously described (27). The expression values of the target genes were normalized with that of GAPDH. A list of gene-specific probes is presented in [supplemental Table S1](#).

FAO activity assay

Cardiac FAO activity was assessed using a commercially available kit (Biomedical Research Service Center, Buffalo, NY) (31). First, 40 mg of cardiac tissue was homogenized with 1 ml of ice-cold cell lysis solution, and 20 µl of the sample was incubated with the control or the reaction solution for 60 min following the manufacturer's protocol. Absorbance at 492 nm was measured using a SpectraMax™ iD3 microplate reader (Molecular Devices), and the FAO activity was determined.

LC-MS

Six mice (three males and three females) from Wt, AKO, and AKO+cHSL groups were used for this analysis. The six mice were divided into two groups (male and female groups). One hundred milligrams of ventricles were excised, and the ventricles from each group were pooled together, followed by lipid extraction using the Bligh-Dyer method (32). The extracted lipids were dried, dissolved in methanol, and subjected to LC-MS analysis performed at Lipidome Lab, Co, Ltd (Akita, Japan).

The samples were separated on an L-column3 C18 metal-free column at 40°C using a gradient solvent system, and electrospray ionization-MS/MS analysis was performed using a Q-Exactive™ Plus mass spectrometer with an UltiMate™

3000 LC system (Thermo Fisher Scientific). Postprocessing of the raw data files for ceramides and DAGs was performed using a lipid molecular identification software Lipid Search™ 4.2.28 (Mitsui Knowledge Industries, Tokyo, Japan). Eighteen species of FFA (C12–C24) were manually analyzed, and the peaks were identified and quantified using the Xcalibur™ Quan Browser software (Thermo Fisher Scientific). *N*-lauroyl-D-erythro-sphingosine (d18:1/12:0), 1,3 diheptadecanoyl-glycerol (d5), and arachidonic acid-d8 were used as the internal standards for ceramide, DAG, and FFA, respectively. The mean values in the male and female groups for each lipid species were compared between genotypes, and the species that showed greater than 2-fold changes between Wt and AKO were extracted.

Life span analysis

Wt mice ($n = 27$; 15 males and 12 females), AKO mice ($n = 22$; 11 males and 11 females), and AKO+cHSL mice ($n = 23$; 10 males and 13 females) were followed for 52 weeks, and the incidence of spontaneous death was recorded as a function of time. Kaplan-Meier plotter analysis was used to analyze the influence of different genetic backgrounds on survival rate. Eleven Wt mice (five males and six females) and 10 AKO+cHSL mice (five males and five females), which survived beyond the 52 weeks, were followed for an additional 26 weeks (total 78 weeks) to compare life span.

Statistical analysis

All values are expressed as the mean \pm SEM. Significance was determined via ANOVA, followed by Fisher's protected least significant difference. $P < 0.05$ was considered significant, and the differences between genotypes are indicated in the figures and tables unless noted otherwise.

RESULTS

Characterization of AKO, cHSL, and AKO+cHSL mice

We first analyzed the protein expression of ATGL and HSL in the cardiac tissues of mice, comparing them between genotypes. As shown in Fig. 1A, AKO and AKO+cHSL mice exhibited no ATGL expression in cardiac tissue. Cardiac HSL expression in cHSL and AKO+cHSL mouse cardiac tissues was markedly greater compared with that in the cardiac tissues of Wt and AKO mice. To assess the phosphorylation status of transgenic HSL, Western blot analyses were performed using specific antibodies against the phosphorylation sites of HSL. As shown in Fig. 1B, transgenic HSL was highly phosphorylated at Ser565 and Ser660 in the cardiac tissues of cHSL and AKO+cHSL mice. The phosphorylation level of Ser563 also tended to be greater in both cHSL mice. As shown in Fig. 1C, the TAG hydrolase activity of cardiac tissue was 66% lower in AKO mice than that in Wt mice. In contrast, the activity in AKO+cHSL mice was 4-fold greater compared with that in AKO mice. Interestingly, the activity in cHSL mice was comparable to that in Wt mice in this assay, suggesting the existence of underlying unknown mechanisms, such as interference

between ATGL and HSL. The activity in heterozygous AKO mice was also comparable to that in Wt mice.

Cardiac HSL overexpression counteracts cardiac steatosis in AKO mice

In order to evaluate the effect of HSL overexpression on cardiac steatosis in AKO mice, we measured cardiac TAG content. The cardiac TAG content of AKO mice was 160-fold greater than that of Wt mice. In contrast, the cardiac TAG content of AKO+cHSL mice was comparable to that of Wt mice (Fig. 1D). The impact of HSL overexpression was also assessed via light microscopy. As shown in Fig. 1E, AKO mice accumulated large LDs in cardiomyocytes, whereas few LDs were observed in the cardiomyocytes of AKO+cHSL mice and Wt mice. We performed electron microscopy in order to observe smaller LDs, potentially overlooked during light microscopy. As shown in the bottom panels of Fig. 1E, very few LDs were observed in the cardiomyocytes of AKO+cHSL mice and Wt cardiomyocytes. Thus, cardiac HSL overexpression conferred protection to AKO mice against cardiac steatosis.

Aberrant expression of PLIN family in AKO heart was normalized in AKO+cHSL mice

We then assessed the expression of the LD-associated PLIN family via Western blot, as we assumed that since huge LDs in AKO mice are associated with PLIN expression changes, HSL overexpression may also exert an impact. As shown in Fig. 2A, AKO mice exhibited greater expression of PLIN2 and PLIN3 than Wt mice. In contrast, AKO+cHSL mice expressed both proteins at levels comparable to those in Wt mice. In contrast to PLIN2 and PLIN3, PLIN5 expression was decreased in AKO relative to that in Wt mice, while comparable between AKO+cHSL and Wt mice. Consistent with the protein expression levels, the mRNA expression of PLIN2 was upregulated while that of PLIN5 was downregulated in AKO mice, whereas the expression levels of both these components were normalized in AKO+cHSL mice (Fig. 2B). Interestingly, the PLIN1 protein was detected in the myocardium following very long exposure, although there was great variation in all genotypes. The PLIN4 protein was undetectable with the antibody used in the current study. Since the phosphorylation of PLINs is crucial for the regulation of lipolysis, we attempted to analyze PLIN1 phosphorylation. However, we could not detect any phosphorylation in PLIN1, as shown in supplemental Fig. S1.

Cardiac HSL overexpression normalized low PG in AKO mice, whereas plasma lipids remained altered in AKO+cHSL mice

Table 1 shows the body weight and plasma concentration of glucose and lipids in mice of the four genotypes. The body weight of male mice was comparable between all four genotypes, while female AKO mice

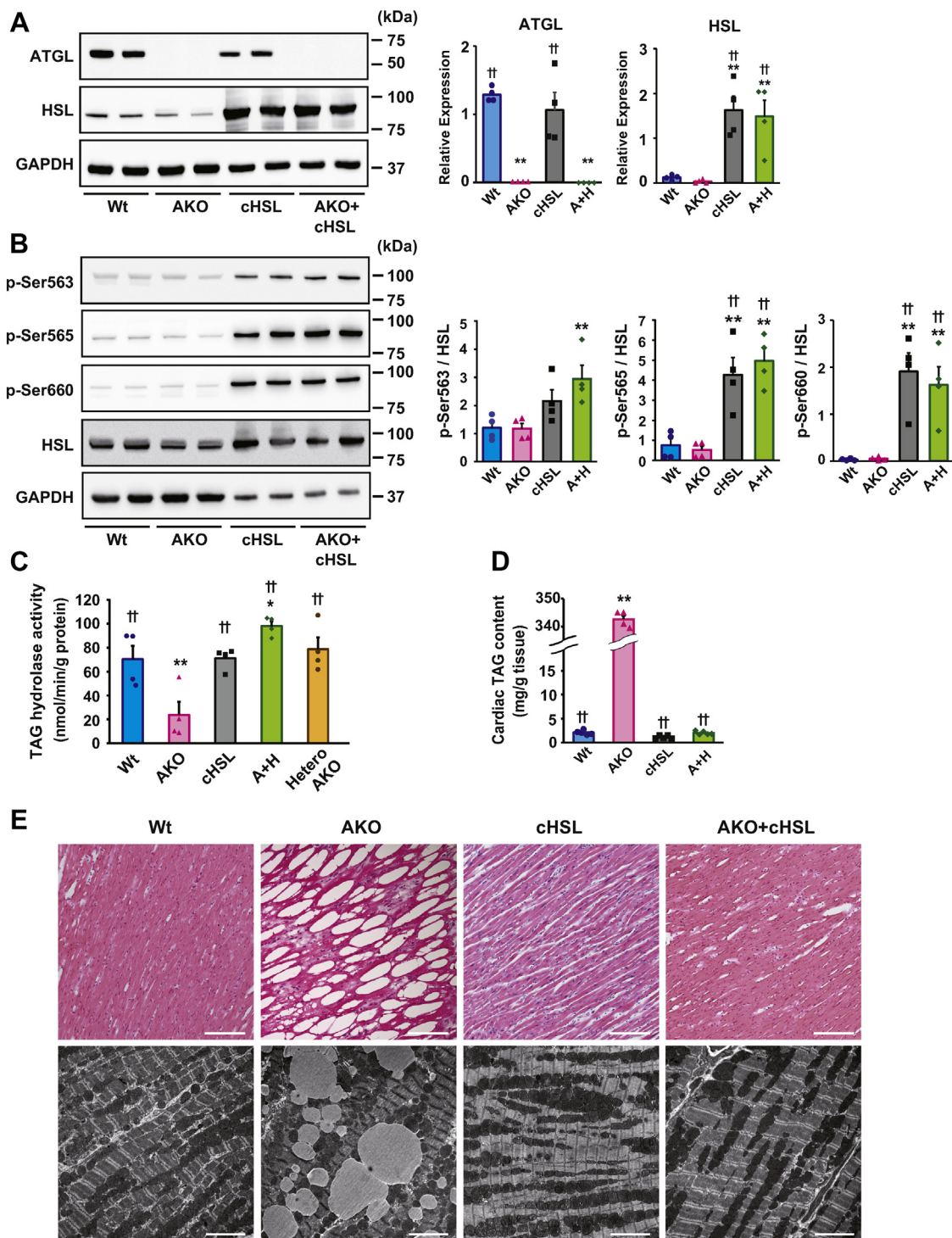


Fig. 1. Generation and characterization of AKO, cHSL, and AKO+cHSL mice. **A:** Protein expression of ATGL and HSL in the cardiac ventricle of Wt, AKO, cHSL, and AKO+cHSL (A+H) mice, as determined via Western blotting using specific antibodies against ATGL or HSL: 10 μ g of the protein sample was subjected to SDS-PAGE, transferred to nitrocellulose membranes, and probed with an appropriate antibody. The graphs present the densitometric analysis of protein expression normalized to that of GAPDH. Values are presented as the mean \pm SEM of four mice/group. **B:** Phosphorylation of HSL using specific antibodies against Ser563, Ser565, and Ser660. Twenty micrograms (Wt and AKO) or 3.3 μ g (cHSL and AKO+cHSL) of the protein sample was subjected to SDS-PAGE, transferred to nitrocellulose membranes, and probed with an appropriate antibody. The graphs present the densitometric analysis of phosphorylated HSLs normalized to total HSL expression. A + H denotes AKO+cHSL mice. Values are presented as the mean \pm SEM of four mice/group. **C:** Cardiac TAG hydrolase activity in Wt, AKO, cHSL, AKO+cHSL (A+H), and heterozygous AKO (hetero AKO) mice. Cardiac ventricles were homogenized in TES buffer containing a protease inhibitor cocktail, and the supernatants were subjected to the assay. Values are presented as the mean \pm SEM of four mice/group. **D:** Cardiac TAG content in Wt, AKO, cHSL, and AKO+cHSL (A+H) mice. Lipids were extracted from cardiac ventricles and quantified as per methods described in the [Materials and Methods](#) section. Values are presented as mean \pm SEM of five (Wt, cHSL, and AKO+cHSL) or four (AKO) mice in

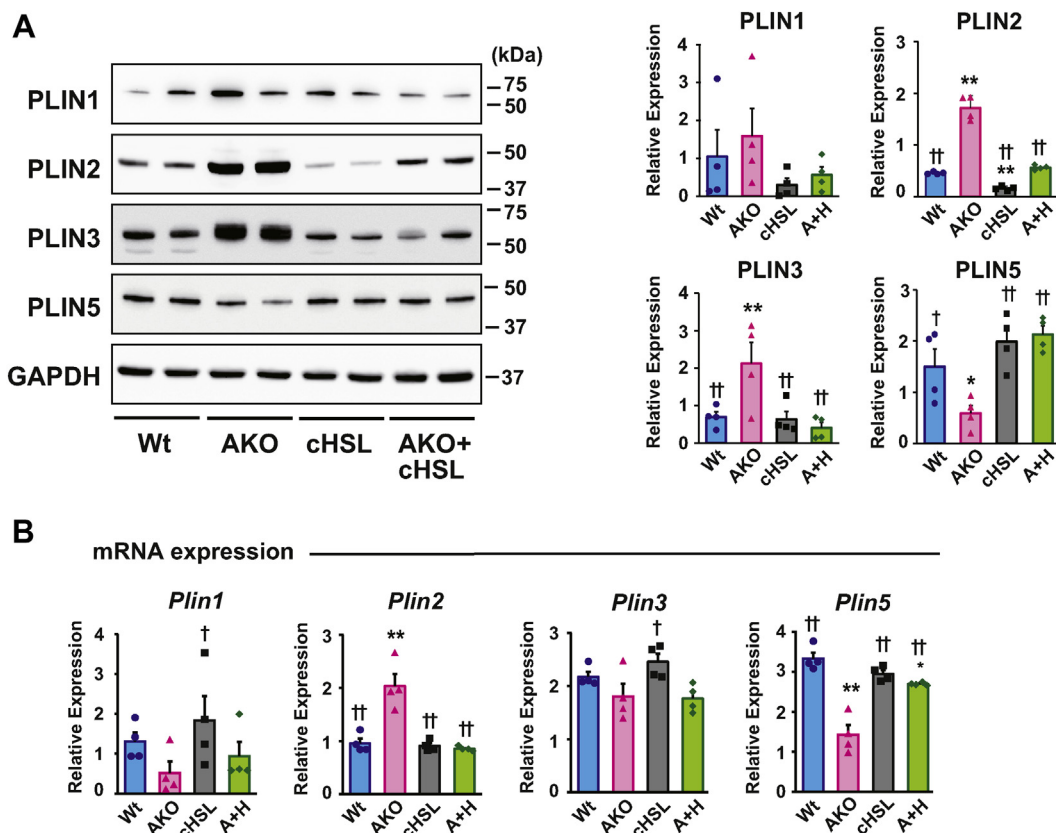


Fig. 2. Expression levels of members of the PLIN family in cardiac tissues. A: Western blot analysis of PLIN1, PLIN2, PLIN3, and PLIN5 in the cardiac ventricles of Wt, AKO, cHSL, and AKO+cHSL (A+H) mice: 20 μ g of protein sample was subjected to SDS-PAGE, transferred to nitrocellulose membranes, and probed with an appropriate antibody. Four mice per group were analyzed, and the representative blots are presented. Note that PLIN1 was detected after an extremely long exposure. The graphs present the densitometric analysis of protein expression normalized to that of GAPDH. Values are presented as the mean \pm SEM of four mice/group. B: mRNA expression levels of PLIN1, PLIN2, PLIN3, and PLIN5 in the cardiac ventricles of Wt, AKO, cHSL, and AKO+cHSL (A+H) mice. The expression levels were determined via RT-qPCR and normalized to GAPDH expression. Values are presented as the mean \pm SEM of four mice per group. * P < 0.05, ** P < 0.01 versus Wt mice; † P < 0.05, †† P < 0.01 versus AKO mice.

were heavier compared with female mice of the other three genotypes. The PG concentration was lower in AKO mice than in Wt mice, as previously reported (33), whereas that of AKO+cHSL mice was similar to that of Wt mice. The plasma concentrations of FFA, TAG, and T-Chol in AKO mice were also lower than those in Wt mice. Interestingly, the plasma FFA concentration of AKO+cHSL mice was between Wt and AKO mice, whereas the plasma TAG concentration remained lower. The plasma T-Chol concentration of AKO+cHSL mice was comparable to that in Wt or cHSL mice.

Cardiac HSL overexpression rescued lethal cardiac dysfunction in AKO mice

We performed echocardiography to analyze the cardiac function of mice. As shown in Table 2, the interventricular septum and left ventricular posterior

wall of AKO mice were thicker than in Wt mice, whereas those of AKO+cHSL mice were once again comparable. Fractional shortening and ejection fraction, which indicate systolic function, were markedly lower in AKO mice compared with Wt mice (25 \pm 2.0% vs. 49 \pm 0.9% and 56 \pm 3.3% vs. 86 \pm 0.7%, respectively). In contrast, the fractional shortening and ejection fraction in AKO+cHSL mice were comparable to those in Wt mice (48 \pm 1.4% vs. 49 \pm 0.9% and 86 \pm 1.1% vs. 86 \pm 0.7%, respectively). The results indicate that cardiac overexpression of HSL completely maintained normal cardiac function in AKO mice.

Abnormal mitochondria and destroyed ICDs were restored by HSL overexpression

In order to determine the cause of cardiac dysfunction in AKO mice, we performed light and electron

each group. E: Representative light (upper panels) and electron (lower panels) micrographs of ventricular tissues derived from Wt, AKO, cHSL, and AKO+cHSL mice. The scale bars represent 100 μ m (upper panels) or 5.0 μ m (lower panels). Five mice per group, three to five sections per mouse were analyzed, and representative images have been presented. * P < 0.05 and ** P < 0.01 versus Wt mice; † P < 0.05 and †† P < 0.01 versus AKO mice.

TABLE 1. Body weight and plasma concentration of glucose and lipids in Wt, AKO, cHSL, and AKO+cHSL mice

Phenotype	Wt	AKO	cHSL	AKO+cHSL
Body weight, male (g)	26.5 ± 0.2	27.1 ± 0.6	26.4 ± 0.6	25.3 ± 0.7
Body weight, female (g)	21.2 ± 0.4 ^a	23.8 ± 0.5 ^b	21.7 ± 0.7 ^c	22.3 ± 0.6
PG (mg/dl)	158 ± 4.5 ^a	112 ± 8.0 ^b	152 ± 6.0 ^a	143 ± 13.6 ^c
FFA (mmol/l)	0.43 ± 0.03 ^a	0.21 ± 0.02 ^b	0.35 ± 0.03 ^a	0.31 ± 0.05 ^{c,d}
TAG (mg/dl)	77 ± 9.9 ^c	50 ± 5.2 ^d	69 ± 7.9	49 ± 4.1 ^d
T-Cho (mg/dl)	71 ± 4.9 ^c	55 ± 3.8 ^d	64 ± 4.9	61 ± 3.4

Data are presented as mean ± SEM of five male and five female mice aged 10–12 weeks.

^a*P* < 0.01 versus AKO mice.

^b*P* < 0.01 versus Wt mice.

^c*P* < 0.05 versus AKO mice.

^d*P* < 0.05 versus Wt mice.

microscopic analyses, focusing on the mitochondria and ICDs of cardiomyocytes. As shown in **Fig. 3B**, clusters of abnormal mitochondria with destroyed cristae were observed in the cardiomyocytes of AKO mice, in contrast to Wt cardiomyocytes wherein round-shaped mitochondria with fine cristae were lined up (**Fig. 3A** and **D**). In AKO cardiomyocytes, some abnormal mitochondria contained vacuoles (**Fig. 3E**). Of note, such abnormal mitochondria were not observed in the cardiomyocytes of AKO+cHSL mice, which harbored normal-shaped mitochondria (**Fig. 3C** and **F**).

ICDs play a critical role in the longitudinal connection of cardiomyocytes, transmission of mechanical force via adherens junctions, and propagation of action potential via gap junctions. As shown in **Fig. 4A**, immunostaining with anti-N-cadherin antibody revealed ICDs as sharp lines under light microscopy in Wt as well as in AKO+cHSL cardiac tissues (**Fig. 4C**). In AKO cardiac tissues, ICDs appeared intact despite expanded cytosol with huge LDs (**Fig. 4B**). However, electron microscopy revealed that some of the ICDs in AKO cardiac tissues appeared loose and with a wider gap (**Fig. 4E**). These loose ICDs contained less adherens junctions, desmosomes, and gap junctions in contrast to the normal ICDs observed in Wt cardiomyocytes (**Fig. 4D**). The ICDs in AKO+cHSL cardiomyocytes appeared sharp and contained clear adherens junctions, desmosomes, and gap junctions (**Fig. 4F**), as observed in Wt cardiomyocytes. High-magnification electron microscopy revealed scarce actin filaments, which reached the adherens junctions, in AKO cardiomyocytes (**Fig. 4H**). In contrast, AKO+cHSL cardiomyocytes had

fine and dense actin filaments connected to the adherens junctions (**Fig. 4I**), as observed for Wt cardiomyocytes (**Fig. 4G**). Thus, microscopic evaluation indicated that the overexpression of HSL completely inhibited mitochondrial malformations and ICD destruction in AKO cardiomyocytes.

Altered expression of PPAR α -regulated genes was partially restored, whereas the expression levels of most genes related to cardiomyopathy were normalized by HSL overexpression

We then analyzed the cardiac mRNA expression of genes related to lipotoxic cardiomyopathy via quantitative RT-PCR. As shown in **Fig. 5A**, the mRNA expression of PPAR α (*Ppara*), which is a key regulator of FAO, was decreased in AKO cardiac tissues, whereas remaining unchanged in AKO+cHSL cardiac tissues. Among PPAR α -regulated genes, the expression of *Cpt1b*, long-chain acyl-CoA dehydrogenase (*Acadl*), medium-chain acyl CoA dehydrogenase (*Acadm*), acyl-CoA oxidase 1 (*Acox1*), uncoupling protein 3 (*Ucp3*), HMG-CoA synthase 2 (*Hmgcs2*), PPAR gamma coactivator 1-alpha (*Ppargc1a*), pyruvate dehydrogenase kinase 4 (*Pdk4*), lipoprotein lipase (*Lpl*), and cluster of differentiation (*Cd36*) was lower, whereas that of uncoupling protein 2 (*Ucp2*) was higher in AKO mice compared with Wt mice. Interestingly, among these altered genes, the expression of *Cpt1b*, *Acadl*, *Acadm*, *Acox1*, and *Ucp3* was the same as Wt levels, whereas *Ucp2*, *Hmgcs2*, *Ppargc1a*, *Pdk4*, *Lpl*, and *Cd36* remained higher or lower in AKO+cHSL mice. Thus, overexpression of HSL maintained the mRNA expression of PPAR α and many of its target genes to the Wt level, with several

TABLE 2. Echocardiographic parameters of Wt, AKO, cHSL, and AKO+cHSL mice

Genotype	HR (beats per minute)	LVIDd (mm)	LVIDs (mm)	IVS (mm)	LVPW (mm)	FS (%)	EF (%)
Wt	658 ± 9	3.1 ± 0.09	1.6 ± 0.07	0.7 ± 0.03	0.7 ± 0.03	49 ± 0.9	86 ± 0.7
AKO	644 ± 19	3.5 ± 0.20 ^a	2.7 ± 0.22 ^b	1.0 ± 0.07 ^b	1.0 ± 0.06 ^b	25 ± 2.0 ^b	56 ± 3.3 ^b
cHSL	633 ± 13	3.2 ± 0.12	1.7 ± 0.08	0.7 ± 0.03	0.7 ± 0.02	47 ± 0.9	85 ± 0.8
AKO+cHSL	638 ± 17	3.0 ± 0.07	1.6 ± 0.08	0.8 ± 0.03	0.8 ± 0.03	48 ± 1.4	86 ± 1.1

EF, ejection fraction; FS, fractional shortening; HR, heart rate; IVS, interventricular septum; LVIDd, left ventricular internal dimension in diastole; LVIDs, left ventricular internal dimension in systole; LVPW, left ventricular posterior wall.

Data are presented as mean ± SEM of 10 male mice aged 10–12 weeks.

^a*P* < 0.01 versus Wt or AKO+cHSL mice.

^b*P* < 0.01 versus Wt, cHSL, or AKO+cHSL mice.

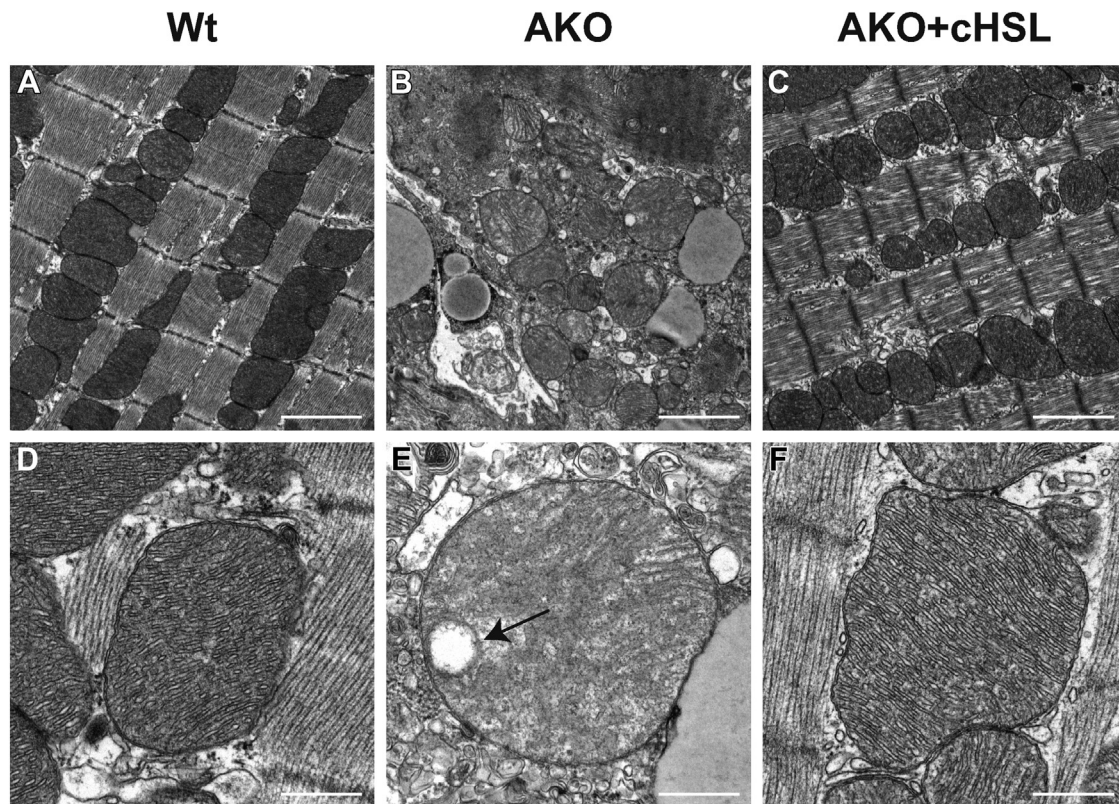


Fig. 3. Representative electron micrographs depicting mitochondrial morphology in the cardiac ventricles of Wt, AKO, and AKO+cHSL mice. Note the cluster of abnormal mitochondria (B) characterized by destroyed cristae and vacuole degeneration (arrow) in the ventricular cardiomyocytes of AKO mice (E), compared with the normal mitochondria presenting with fine cristae observed in the ventricular cardiomyocytes of Wt (A, D) or AKO+cHSL mice (C, F). Four mice per group, three to five sections per mouse were analyzed, and representative images under low magnification (A, B, and C) or high magnification (D, E, and F) have been presented. The scale bars in the upper panels represent 2 μm ; the scale bars in the lower panels represent 0.5 μm .

PPAR α -regulated genes altered in AKO+cHSL mice. To assess whether this partial recovery of the expression levels of PPAR α -regulated genes improves cardiac FAO capability, we analyzed cardiac FAO activity using cardiac tissue homogenates. As shown in [supplemental Fig. S2](#), cardiac FAO activity in AKO mice was significantly lower than that in Wt mice, whereas that in AKO+cHSL mice was comparable to that in Wt mice. Thus, the partial recovery of the expression levels of PPAR α -regulated genes by HSL overexpression seemed to normalize cardiac FAO capability.

We further analyzed the expression of genes related to TAG synthesis (*Gpam*, *Ppap2a*, *Dgat1*, and *Dgat2*), macrophage (*Ccl2*, *Msr1*, and *Mrc1*), inflammation (*Tnf*, *Il1b*, and *Il6*), fibrosis (*Tgfb1*, *Tgfb2*, and *Col1a1*), cardiac stress (*Nppa* and *Nppb*), apoptosis (*Bcl2*, *Bax*, and *Casp9*), and antioxidant proteins, metallothioneins (*Mt1* and *Mt2*). As shown in [Fig. 5B](#), the expression of *Ppap2a* was upregulated in AKO mice, whereas it was comparable to Wt mice in AKO+cHSL mice. The expression of *Dgat2* was downregulated in AKO mice, whereas it was similar to Wt mice in AKO+cHSL mice. As shown in [Fig. 5C and D](#), macrophage-related and inflammation-related genes were significantly upregulated in AKO mice compared with Wt mice, whereas similar in

AKO+cHSL mice, suggesting the presence of macrophage infiltration and inflammation in AKO cardiac tissues but not in AKO+cHSL cardiac tissues. Genes related to fibrosis and cardiac stress were also upregulated in AKO mice compared with Wt mice, while remaining at Wt levels in AKO+cHSL mice ([Fig. 5E and F](#)). Apoptosis-related *Bax* and *Bcl2* as well as antioxidant *Mt1* and *Mt2* expression was higher in AKO mice, whereas remaining at Wt levels in AKO+cHSL mice ([Fig. 5G and H](#)).

Macrophage infiltration, fibrosis, and apoptosis were present in the cardiac tissue of AKO mice, whereas they were absent in AKO+cHSL mice

Since the cardiac gene expression profile indicated potential macrophage infiltration, fibrosis, and apoptosis in AKO cardiac tissues, we investigated these features via immunohistochemistry. As shown in [Fig. 6B](#), a number of F4/80-positive macrophages were detected in AKO cardiac tissues, whereas rarely observed in Wt ([Fig. 6A](#)) or AKO+cHSL cardiac tissues ([Fig. 6C](#)). Since macrophages scavenge modified lipoproteins, we aimed to determine whether macrophages infiltrated cardiomyocytes and directly targeted LDs in AKO cardiac tissues. To this end, we performed double

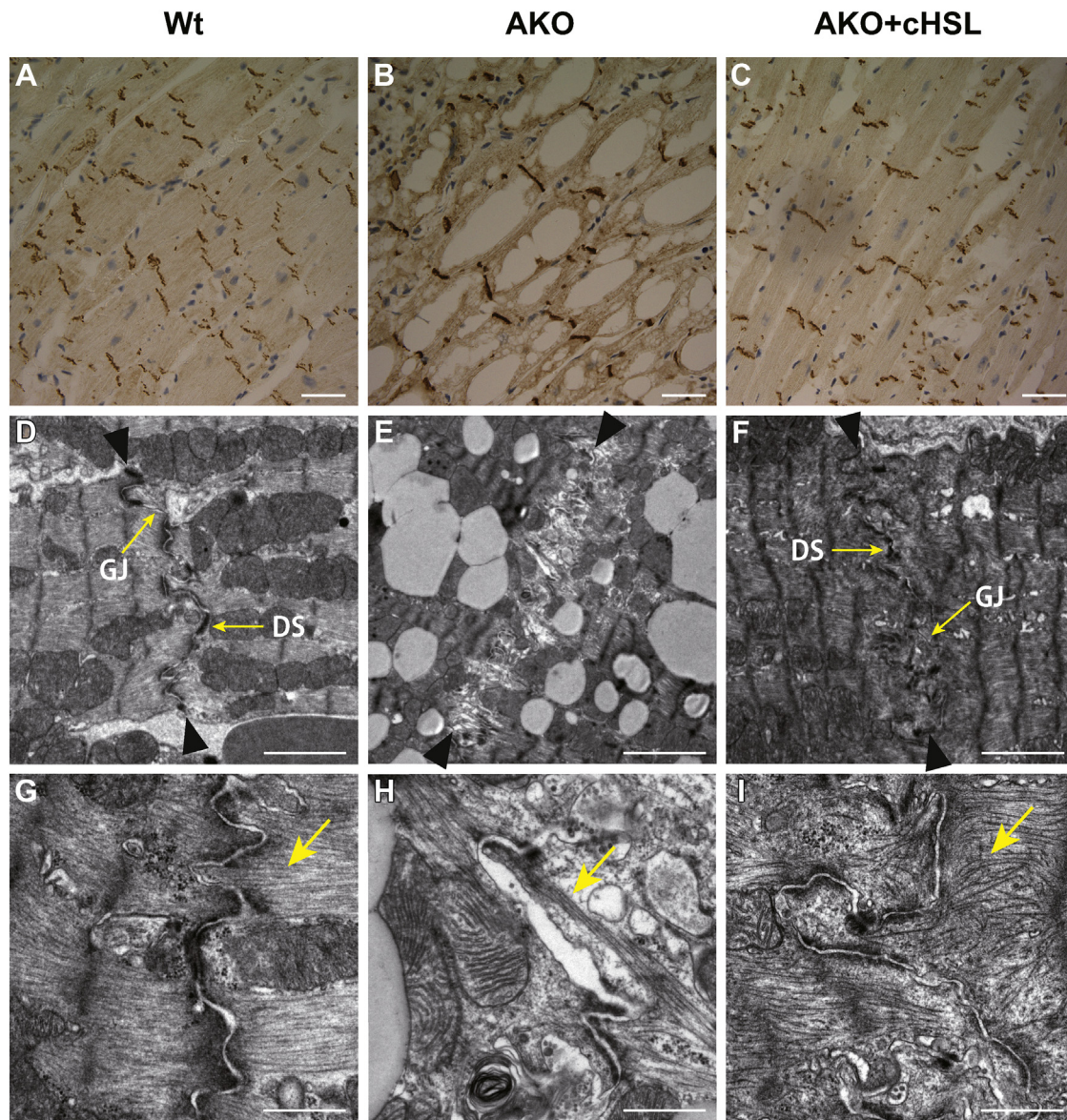


Fig. 4. ICDs in mouse cardiac ventricles. A–C: Representative light micrographs of the cardiac ventricles of Wt (A), AKO (B), and AKO+cHSL (C) mice. ICDs were subjected to immunostaining procedures with a specific antibody against N-cadherin. The scale bars represent 20 μ m. D–F: Representative electron low-magnification micrographs showing ICDs between the arrowheads. Note the wider gap in ICDs of AKO mice (E) compared with that observed in Wt (D) or AKO+cHSL (F) mice. DS indicates desmosomes, and GJ indicates gap junctions. The scale bars represent 5 μ m. G–I: Representative electron high-magnification micrographs showing actin filaments (arrows) connected to adherence junctions at ICD. Note the scarce actin filaments in the cardiomyocytes of AKO mice (H), compared with the fine and dense filaments observed in the cardiomyocytes of Wt (G) or AKO+cHSL (I) mice. The scale bars represent 0.5 μ m. Four mice per group, three to five sections per mouse were analyzed, and representative images have been presented.

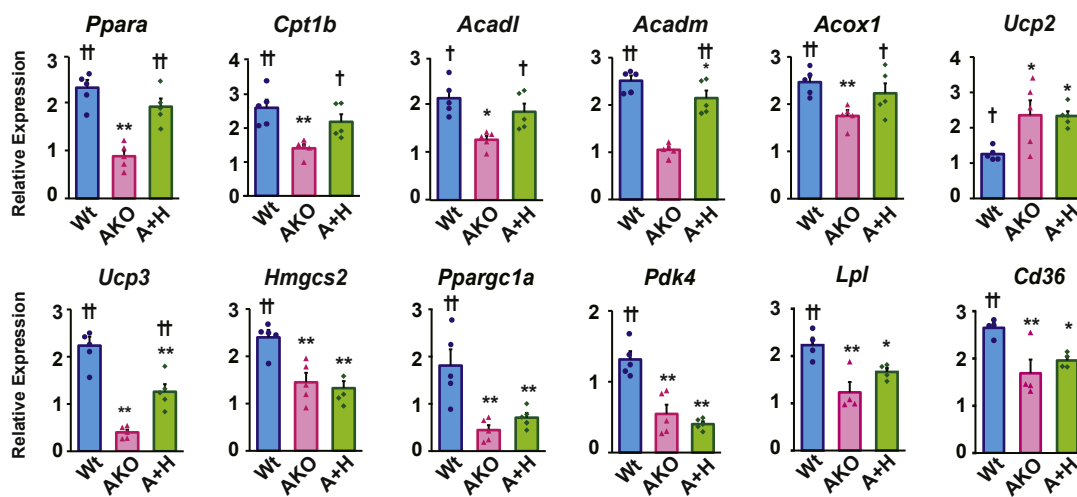
staining using antibodies against F4/80 and PLIN2. The results indicated that no F4/80-positive macrophages interacted with the LD surface, instead localizing within the cardiac interstitium (Fig. 6E). We also performed Masson's trichrome staining to assess cardiac fibrosis, which was markedly greater in AKO cardiac tissues (Fig. 6H) compared with that observed in cardiac tissues of Wt mice (Fig. 6G) or AKO+cHSL mice (Fig. 6I). TUNEL staining indicated a significant increase in apoptotic cells within AKO cardiac tissues (1.64 apoptotic cells/high-power field, Fig. 6K), whereas no

apoptotic cells were detected in Wt or AKO+cHSL cardiac tissues (Fig. 6J and L).

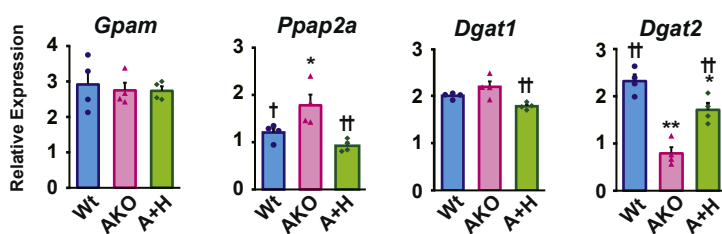
Cardiac content of ceramide and DAG species was markedly increased in AKO mice, whereas normalized in AKO+cHSL mice

In order to address the pathogenesis of apoptosis and inflammation observed in AKO cardiac tissues, we performed a lipidomic analysis using cardiac lipids extracted from Wt, AKO, and AKO+cHSL mice. The lipidomic analysis identified totally 38 species of

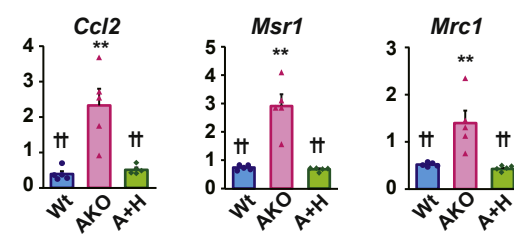
A PPAR α -regulated genes



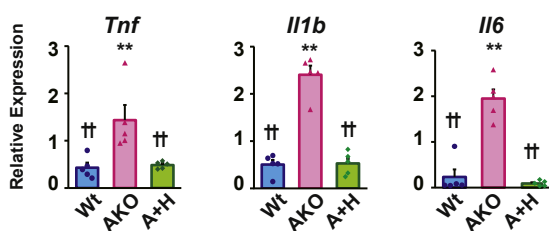
B TAG synthesis



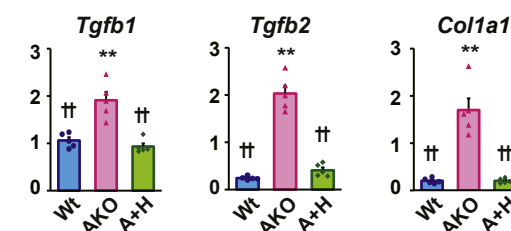
C Macrophage



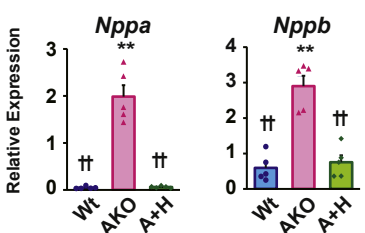
D Inflammation



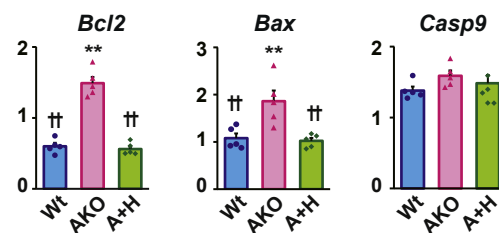
E Fibrosis



F Cardiac stress



G Apoptosis



H Antioxidants

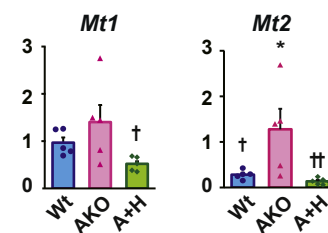


Fig. 5. Cardiac expression of genes related to PPAR α (A), TAG synthesis (B), macrophage (C), inflammation (D), fibrosis (E), cardiac stress (F), apoptosis (G), and antioxidants (H). Total RNA was extracted from the ventricles of Wt, AKO, and AKO+cHSL (A+H) mice, and the mRNA expression levels were determined via RT-qPCR and normalized to GAPDH expression. Values are presented as mean \pm SEM of five mice per group. * P < 0.05, ** P < 0.01 versus Wt mice; † P < 0.05, †† P < 0.01 versus AKO mice. *Acadl*, long-chain specific acyl-CoA dehydrogenase; *Acadm*, middle-chain specific acyl-CoA dehydrogenase; *Acox1*, acyl-CoA oxidase 1; *Ccl2*, C-C motif chemokine 2/monocyte chemoattractant protein 1; *Col1a1*, collagen type 1 alpha 1; *Gpam*, glycerol-3-phosphate acyltransferase, mitochondrial; *Hmgcs2*, HMG-CoA synthase 2; *Mrc1*, mannose receptor c-type 1; *Msr1*, macrophage scavenger receptor 1; *Mt1*, metallothionein 1; *Mt2*, metallothionein 2; *Nppa*, natriuretic peptide type A; *Nppb*, natriuretic peptide type B; *Pdk4*, pyruvate dehydrogenase kinase 4; *Ppap2a*, phosphatidic acid phosphatase type 2A; *Ppargc1a*, PPAR gamma coactivator 1 alpha.

ceramide in the cardiac tissues of the mice investigated. As shown in [Fig. 7A](#) and [supplemental Table S2](#), whereas total cardiac ceramide content in AKO mice

was comparable to that in Wt mice, 12 species of ceramides were increased greater than 2-fold in AKO mice compared with those in Wt mice. In contrast, all

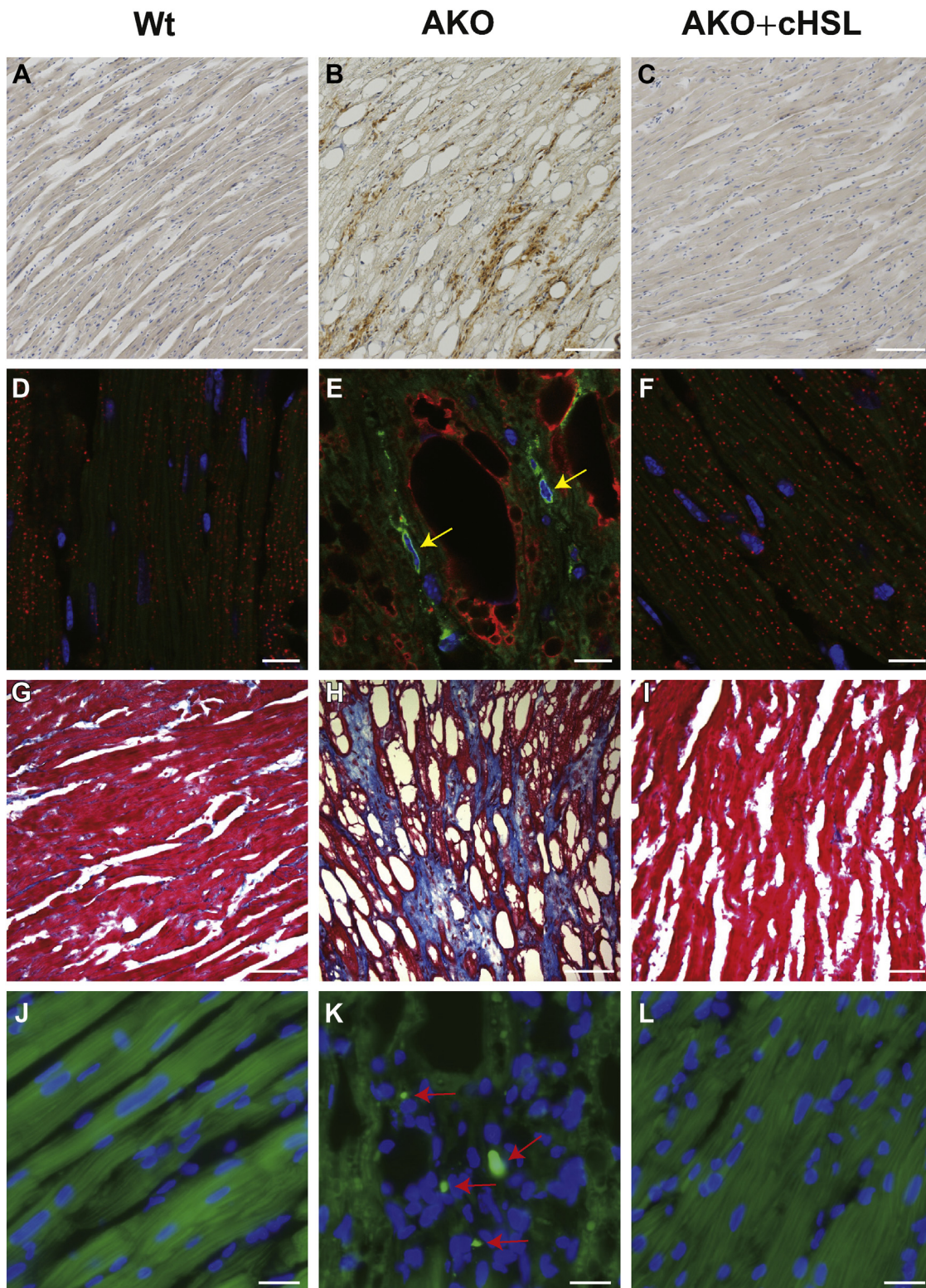


Fig. 6. Cardiac macrophage infiltration, interstitial fibrosis, and apoptosis. A–C: Representative light micrographs of cardiac ventricles derived from Wt, AKO, and AKO+cHSL mice. Macrophages were immunostained with a specific antibody against F4/80. The scale bars represent 100 μ m. D–F: Macrophage localization in cardiac ventricles. Tissue sections were subjected to immunostaining procedures with a specific antibody against F4/80 and PLIN2, and they were analyzed via confocal microscopy. Representative images are presented showing macrophages (indicated in green, with arrows), the LD surface (indicated in red), and the nucleus (indicated in blue). The scale bars represent 10 μ m. G–I: Representative light micrographs of cardiac ventricles derived from Wt, AKO, and AKO+cHSL mice subjected to staining procedures with Masson's trichrome staining. The scale bars represent 100 μ m. J–L: Apoptotic cells in cardiac ventricles of Wt, AKO, and AKO+cHSL mice. DNA fragmentation was detected using the TUNEL assay, and representative images have been presented. TUNEL-positive nuclei are shown in green (with arrows). The scale bars represent 20 μ m. Five mice per group were selected, two sections per mouse were analyzed, and representative images have been presented.

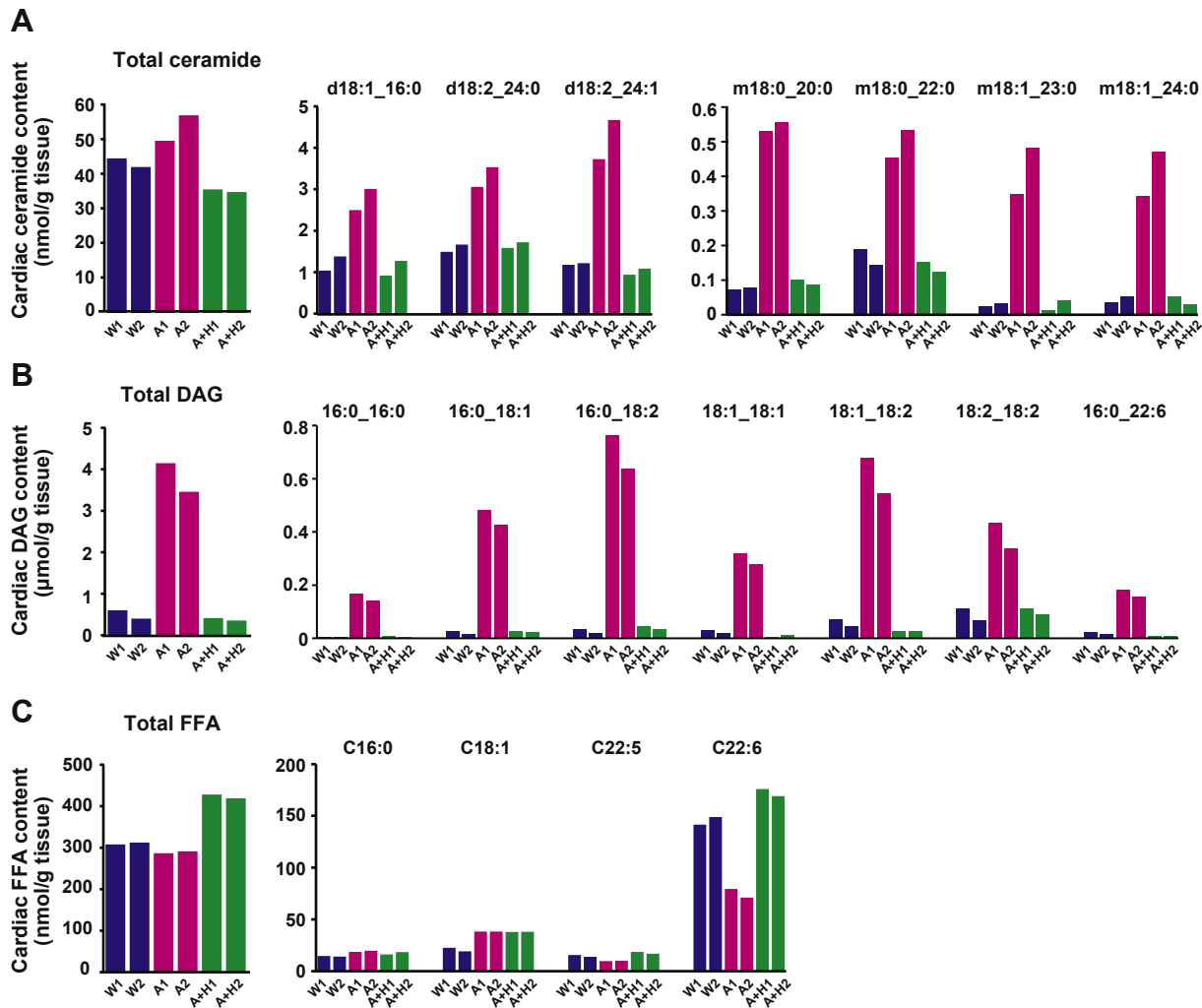


Fig. 7. Ventricular lipidomic analysis for ceramide, DAG, and FFA contents. Six mice (three males and three females) from Wt, AKO, and AKO+cHSL (A+H) groups were divided into two groups (male and female groups), and 100 mg of ventricles from each mouse were excised. The ventricles from each group were pooled together, and lipids were extracted. The extracted lipids were then dried, dissolved in methanol, and subjected to LC-MS analysis as described in the [Materials and Methods](#) section. The mean values in the male and female groups for each lipid species were compared between genotypes, and the species that showed greater than 2-fold changes between Wt and AKO were extracted. The abundant species of ceramide (A) and DAG (B) or the predominant species of FFA (C) are presented. A1, male AKO; A2, female AKO; A+H1, male AKO+cHSL; A+H2, female AKO+cHSL group; W1, male Wt; W2, female Wt. Detailed data are presented in [supplemental Tables S2–S4](#).

ceramide species in AKO+cHSL mice were comparable to those in Wt mice. The lipidomic analysis identified totally 98 species of DAG in the cardiac tissues of the mice. Among these species, 79 species were increased greater than 2-fold in AKO mice compared with those in Wt mice ([supplemental Table S3](#)). As shown in [Fig. 7B](#), the total DAG content in AKO mice was 8-fold greater compared with that in Wt mice, and many DAG species were extremely increased in AKO mice. In contrast, in AKO+cHSL mice, most of the increased DAG species were at a comparable level with those in Wt mice. As shown in [Fig. 7C](#) and [supplemental Table S4](#), the total cardiac content of FFA in AKO mice was comparable to that in Wt mice, whereas it was 37% greater in AKO+cHSL mice compared with that in Wt mice. Of note, the cardiac content of EPA (C22:5) was 36% (vs. Wt) or 48% (vs. AKO+cHSL) lower in AKO

mice, and the content of DHA (C22:6) was 49% (vs. Wt) or 57% (vs. AKO+cHSL) lower in AKO mice. Thus, the results of the lipidomic analysis revealed that increased toxic lipids (ceramide and DAG) and decreased ω -3 FAs (EPA and DHA) might be related to the pathogenesis of lipotoxic cardiomyopathy in AKO mice, and HSL overexpression normalizes this aberrant condition.

Cardiac HSL overexpression rescues AKO mice from cardiac death

Finally, we studied the effect of HSL overexpression on the life span of AKO mice. As shown in [Fig. 8](#), most AKO mice died within 16 weeks, whereas all AKO+cHSL mice studied lived for 52 weeks. We further followed 11 Wt mice (five males and six females) and 10 AKO+cHSL mice (five males and five females) until 78 weeks of age. Neither AKO+cHSL

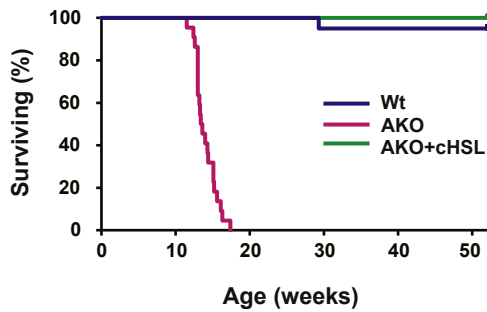


Fig. 8. Life span analysis. Wt mice ($n = 27$; 15 males and 12 females), AKO mice ($n = 22$; 11 males and 11 females), and AKO+cHSL mice ($n = 23$; 10 males and 13 females) were subjected to follow-up for 52 weeks, and the incidence of spontaneous death was recorded as a function of time. Differences between survival curves were compared using Kaplan-Meier survival analysis.

mice nor Wt mice died within this follow-up period. Thus, the premature death of AKO mice was completely prevented via the cardiac overexpression of HSL.

DISCUSSION

In the present study, we demonstrated that cardiac-specific HSL overexpression completely inhibited lipotoxic cardiomyopathy and protected AKO mice from cardiac death.

The precise mechanism through which impaired FAO leads to end-stage heart failure in AKO mice remains unclear (6, 34). We observed higher inflammatory cytokine expression, macrophage infiltration, cardiomyocyte apoptosis, transforming growth factor beta expression, and fibrosis in AKO cardiac tissues, all of which indicated the occurrence of chronic inflammation. In addition, a lipidomic analysis revealed a marked increase of ceramide and DAG species and decrease of ω -3 FAs in the ventricle of AKO mice (Fig. 7). Thus, one possible pathophysiological mechanism of lipotoxic cardiomyopathy in AKO cardiac tissues is that impaired FAO caused by disrupted LD lipolysis induces mitochondrial stress, monocyte chemotactic protein 1 expression, and apoptosis, which are associated with ceramide and DAG accumulation, leading to macrophage infiltration and the recruitment of other inflammatory cells. These events in turn lead to chronic inflammation and, eventually, interstitial fibrosis (35, 36).

Recent advances in LD research have revealed that LDs interact with intracellular organelles, including the ER, lysosomes, peroxisomes, and mitochondria. Associated with many proteins, LDs play an important role in protecting cells from lipotoxicity and oxidative stress through the regulation of ER stress, mitochondrial damage, and autophagy (1). Considering the aberrant size and shape of LDs in AKO cardiomyocytes, their protective functions might be

impaired, which results in ER stress, autophagy defects, and apoptosis, in turn triggering cytokine secretion and chronic inflammation.

Based on the current results, cardiac overexpression of HSL in AKO mice appeared not only to restore the lipolytic cascade but also to normalize mitochondrial FAO and prevent proinflammatory/proapoptotic conditions. We previously reported that, despite conditions of increased FAO, cardiac overexpression of HSL eliminates LDs in the cardiac tissues of diabetic mice without inducing intracellular lipotoxicity (27). Taken together with the current findings, these suggest that FAs released by overexpressed HSL appear to be oxidized smoothly within the mitochondria or released out of the cell via FA transporters (i.e., FA-binding proteins) without generating intracellular lipotoxicity (37, 38).

The downregulation of PPAR α -regulated genes is also critical for impaired FAO and mitochondrial dysfunction in AKO cardiac tissues (17). Our results indicated that various genes implicated in FAO, including *Cpt1b*, *Acadl*, *Acadm*, *Acox1*, and *Ucp3*, were downregulated in AKO cardiac tissues (Fig. 5). HSL overexpression maintained the expression of these, whereas other PPAR α -regulated genes, including *Ucp2*, *Hmgcs2*, *Pprgc1a*, *Pdk4*, *Lpl*, and *Cd36*, remained altered in AKO+cHSL cardiac tissues. This discrepancy might be due to the substrate specificity or preferences of ATGL and HSL. The two lipases possess distinct functions in the catabolism of TAG estolides (39). Furthermore, HSL hydrolyzes retinol esters, which regulate gene expression (40), as well as DAGs, which are involved in cellular signaling (25, 41). Our results indicate that HSL generates sufficient PPAR α ligands for the maintenance of FAO and mitochondrial function in the AKO cardiac tissue.


Altered PLIN expression might also affect the activity of HSL in AKO cardiac tissues. PLIN5 is mainly expressed in cardiomyocytes, skeletal muscle cells, and brown adipocytes, whereas PLIN2 is ubiquitously expressed (42). We observed an upregulation of PLIN2 and a downregulation of PLIN5 in AKO cardiac tissues (Fig. 2A and B). As it has been reported that PLIN2-rich LDs are catabolized more efficiently by HSL than PLIN5-rich LDs (43), it is possible that LDs with a high PLIN2/PLIN5 ratio in AKO cardiac tissues might have been catabolized efficiently under HSL overexpression conditions. Taken together, cardiac-specific HSL overexpression in AKO mice maintained normal FAO and mitochondrial function by restoring the lipolytic cascade and PPAR α function without the generation of intracellular lipotoxicity, thus preventing macrophage infiltration, inflammation, and cardiac fibrosis. As a result, AKO mice exhibited normal cardiac function and had a normal life span.

The reason underlying the massive accumulation of TAG in AKO cardiac tissues despite endogenous HSL expression remains unclear. It is apparent that basal levels of HSL are unable to initiate the lipolytic cascade

in the absence of ATGL in the cardiac tissue, in contrast to adipose tissues wherein TAG accumulates modestly (22). The trivial expression of PLIN1 might be one of the reasons why endogenous HSL is inactive as a TAG lipase within the cardiac tissue (44). Considering these phenotypes of AKO mice, we expected a limited ATGL compensation via HSL overexpression. However, the observed compensation was greater than expected, as AKO+cHSL mice demonstrated normal cardiac TAG content. According to a report by Schweiger *et al.* (45), the TAG lipase activity of HSL is approximately one-seventh that of ATGL during *in vitro* hydrolase assays. The present study revealed 4-fold greater cardiac TAG hydrolase activity in AKO+cHSL mice compared with that in AKO mice (Fig. 1C). Importantly, our findings indicated that exogenous HSL could function as a TAG lipase even in the absence of ATGL within the cardiac tissue and suggests that this level of HSL activation might be a practical target when applied to clinical settings. In addition, given that the cardiac HSL (cholesterol esterase) activity in cHSL mice is 8-fold greater than that in Wt mice (27), the cardiac DAG hydrolase activity might also be similarly greater in AKO+cHSL mice, resulting in a normal cardiac DAG content in AKO+cHSL mice.

Currently, gene therapy through viral vectors has been introduced for the treatment of various genetic disorders. Adeno-associated viruses (AAVs) are mainly used as vectors, since these are suitable for gene transfer to the retina, liver, and muscles (46). Even though several safety issues of AAVs remain to be addressed (47), AAV-based gene therapies have been approved for LPL deficiency, inherited retinal diseases, and spinal muscular atrophy in the United States and Europe (48–50). Although introducing the ATGL gene is the default option in gene therapy, considering the immune response against foreign proteins, gene transfer of HSL might be relatively safer compared with that of the ATGL gene in ATGL-deficient patients (47, 51). In addition, HSL overexpression has been shown to induce no lipotoxicity in adipose tissue or liver in mice (52, 53). Therefore, targeting HSL is a promising novel therapeutic strategy for ATGL deficiency-associated lipotoxic cardiomyopathy.

Data availability

Data are available on request to Jinya Suzuki (Third Department of Internal Medicine, University of Fukui, Faculty of Medical Sciences; E-mail: jinya@u-fukui.ac.jp). 

Supplemental data

This article contains [supplemental data](#).

Acknowledgments

The authors give special thanks to F. Kitaguchi for skillful technical assistance. They also thank J. Yamamoto and H. Takagi (Life Science Research Laboratory, University of

Fukui) for performing the confocal and electron microscopy.

Author contributions

J. S. conceptualization; M. Y. and J. S. methodology; Y. Z., R. S., and T. K. validation; M. Y., J. S., and S. S. investigation; M. Y. and J. S. writing—original draft; M. Y., J. S., S. S., Y. Z., R. S., T. K., F. B. K., and T. I. writing—review & editing; F. B. K. and T. I. supervision.

Author ORCIDiDs

Jinya Suzuki  <https://orcid.org/0000-0002-5670-3528>

Fredric B. Kraemer  <https://orcid.org/0000-0003-2468-7807>

Tamotsu Ishizuka  <https://orcid.org/0000-0002-8347-3553>

Funding and additional information

This work was supported by research grants from the University of Fukui (to M. Y.); the Ministry of Education, Culture, Sports, Science and Technology in Japan (to J. S.; grant number: 26461360); and the National Institute of Diabetes and Digestive and Kidney Diseases grant (to F. B. K.; grant number: P30 DK-116074).

Conflict of interest

The authors declare that they have no conflicts of interest with the contents of this article.

Abbreviations

AAV, adeno-associated virus; AKO, ATGL-KO; AKO+cHSL, ATGL knockout with cardiac-specific HSL overexpression; ATGL, adipose triglyceride lipase; cHSL, cardiac-specific HSL-overexpressing mice; CPT, carnitine palmitoyltransferase; DAG, diacylglycerol; ER, endoplasmic reticulum; FAO, FA oxidation; HSL, hormone-sensitive lipase; ICD, intercalated disc; LD, lipid droplet; LV, left ventricular; MAG, monoacylglycerol; NLSDM, neutral lipid storage disease with myopathy; PG, plasma glucose; PLIN, perilipin; TAG, triacylglycerol; T-Chol, total cholesterol; TES, 20 mM Tris, 1 mM EDTA, 255 mM sucrose, pH 7.4 buffer.

Manuscript received August 27, 2021, and in revised form March 3, 2022. Published, JLR Papers in Press, March 11, 2022, <https://doi.org/10.1016/j.jlr.2022.100194>

REFERENCES

1. Olzmann, J. A., and Carvalho, P. (2019) Dynamics and functions of lipid droplets. *Nat. Rev. Mol. Cell Biol.* **20**, 137–155
2. Nakamura, M., and Sadoshima, J. (2020) Cardiomyopathy in obesity, insulin resistance and diabetes. *J. Physiol.* **598**, 2977–2993
3. Dirks, E., Schwenk, R. W., Glatz, J. F., Luiken, J. J., and van Eys, G. J. (2011) High fat diet induced diabetic cardiomyopathy. *Prostaglandins Leukot. Essent. Fatty Acids.* **85**, 219–225
4. Unger, R. H., and Orci, L. (2001) Diseases of liporegulation: new perspective on obesity and related disorders. *FASEB J.* **15**, 312–321
5. Park, T. S., and Goldberg, I. J. (2012) Sphingolipids, lipotoxic cardiomyopathy, and cardiac failure. *Heart Fail. Clin.* **8**, 633–641
6. Drosatos, K., and Schulze, P. C. (2013) Cardiac lipotoxicity: molecular pathways and therapeutic implications. *Curr. Heart Fail. Rep.* **10**, 109–121
7. Holland, W. L., and Summers, S. A. (2008) Sphingolipids, insulin resistance, and metabolic disease: new insights from *in vivo*

- manipulation of sphingolipid metabolism. *Endocr. Rev.* **29**, 381–402
8. Goldberg, I. J., Trent, C. M., and Schulze, P. C. (2012) Lipid metabolism and toxicity in the heart. *Cell Metab.* **15**, 805–812
 9. Magoulas, P. L., and El-Hattab, A. W. (2012) Systemic primary carnitine deficiency: an overview of clinical manifestations, diagnosis, and management. *Orphanet J. Rare Dis.* **7**, 68
 10. Tripp, M. E., Katcher, M. L., Peters, H. A., Gilbert, E. F., Arya, S., Hodach, R. J., and Shug, A. L. (1981) Systemic carnitine deficiency presenting as familial endocardial fibroelastosis: a treatable cardiomyopathy. *N. Engl. J. Med.* **305**, 385–390
 11. North, K. N., Hoppel, C. L., De Girolami, U., Kozakewich, H. P., and Korson, M. S. (1995) Lethal neonatal deficiency of carnitine palmitoyltransferase II associated with dysgenesis of the brain and kidneys. *J. Pediatr.* **127**, 414–420
 12. Rinaldo, P., Matern, D., and Bennett, M. J. (2002) Fatty acid oxidation disorders. *Annu. Rev. Physiol.* **64**, 477–502
 13. Cheng, L., Ding, G., Qin, Q., Huang, Y., Lewis, W., He, N., Evans, R. M., Schneider, M. D., Brako, F. A., Xiao, Y., Chen, Y. E., and Yang, Q. (2004) Cardiomyocyte-restricted peroxisome proliferator-activated receptor-delta deletion perturbs myocardial fatty acid oxidation and leads to cardiomyopathy. *Nat. Med.* **10**, 1245–1250
 14. He, L., Kim, T., Long, Q., Liu, J., Wang, P., Zhou, Y., Ding, Y., Prasain, J., Wood, P. A., and Yang, Q. (2012) Carnitine palmitoyltransferase-1b deficiency aggravates pressure overload-induced cardiac hypertrophy caused by lipotoxicity. *Circulation.* **126**, 1705–1716
 15. Zimmermann, R., Strauss, J. G., Haemmerle, G., Schoiswohl, G., Birner-Gruenberger, R., Riederer, M., Lass, A., Neuberger, G., Eisenhaber, F., Hermetter, A., and Zechner, R. (2004) Fat mobilization in adipose tissue is promoted by adipose triglyceride lipase. *Science.* **306**, 1383–1386
 16. Zechner, R., Madeo, F., and Kratky, D. (2017) Cytosolic lipolysis and lipophagy: two sides of the same coin. *Nat. Rev. Mol. Cell Biol.* **18**, 671–684
 17. Haemmerle, G., Moustafa, T., Woelkart, G., Büttner, S., Schmidt, A., van de Weijer, T., Hesselink, M., Jaeger, D., Kienesberger, P. C., Zierler, K., Schreiber, R., Eichmann, T., Kolb, D., Kotzbeck, P., Schweiger, M., et al. (2011) ATGL-mediated fat catabolism regulates cardiac mitochondrial function via PPAR- α and PGC-1. *Nat. Med.* **17**, 1076–1085
 18. Missaglia, S., Coleman, R. A., Mordente, A., and Tavian, D. (2019) Neutral lipid storage diseases as cellular model to study lipid droplet function. *Cells.* **8**, 187
 19. Reilich, P., Horvath, R., Krause, S., Schramm, N., Turnbull, D. M., Trenell, M., Hollingsworth, K. G., Gorman, G. S., Hans, V. H., Reimann, J., MacMillan, A., Turner, L., Schollen, A., Witte, G., Czermin, B., et al. (2011) The phenotypic spectrum of neutral lipid storage myopathy due to mutations in the PNPLA2 gene. *J. Neurol.* **258**, 1987–1997
 20. Hirano, K., Ikeda, Y., Zaima, N., Sakata, Y., and Matsumiya, G. (2008) Triglyceride deposit cardiomyovascularopathy. *N. Engl. J. Med.* **359**, 2396–2398
 21. Higashi, M., Hirano, K., Kobayashi, K., Ikeda, Y., Issiki, A., Otsuka, T., Suzuki, A., Yamaguchi, S., Zaima, N., Hamada, S., Hanada, H., Suzuki, C., Nakamura, H., Nagasaka, H., Miyata, T., et al. (2015) Distinct cardiac phenotype between two homozygotes born in a village with accumulation of a genetic deficiency of adipose triglyceride lipase. *Int. J. Cardiol.* **192**, 30–32
 22. Haemmerle, G., Lass, A., Zimmermann, R., Gorkiewicz, G., Meyer, C., Rozman, J., Heldmaier, G., Maier, R., Theussl, C., Eder, S., Kratky, D., Wagner, E. F., Klingenspor, M., Hoefler, G., and Zechner, R. (2006) Defective lipolysis and altered energy metabolism in mice lacking adipose triglyceride lipase. *Science.* **312**, 734–737
 23. van de Weijer, T., Havekes, B., Bilet, L., Hoeks, J., Sparks, L., Bosma, M., Pagliarunga, S., Jorgensen, J., Janssen, M. C., Schaart, G., Sauerwein, H., Smeets, J. L., Wildberger, J., Zechner, R., Schrauwen-Hinderling, V. B., et al. (2013) Effects of bezafibrate treatment in a patient and a carrier with mutations in the PNPLA2 gene, causing neutral lipid storage disease with myopathy. *Circ. Res.* **112**, e51–e54
 24. Suzuki, A., Yamaguchi, S., Li, M., Hara, Y., Miyauchi, H., Ikeda, Y., Zhang, B., Higashi, M., Ikeda, Y., Takagi, A., Nagasaka, H., Kobayashi, K., Magata, Y., Aoyama, T., and Hirano, K. I. (2018) Tricaprin Rescues Myocardial Abnormality in a Mouse Model of Triglyceride Deposit Cardiomyovascularopathy. *J. Oleo Sci.* **67**, 983–989
 25. Haemmerle, G., Zimmermann, R., Hayn, M., Theussl, C., Waeg, G., Wagner, E., Sattler, W., Magin, T. M., Wagner, E. F., and Zechner, R. (2002) Hormone-sensitive lipase deficiency in mice causes diglyceride accumulation in adipose tissue, muscle, and testis. *J. Biol. Chem.* **277**, 4806–4815
 26. Fredrikson, G., Strålfors, P., Nilsson, N. O., and Belfrage, P. (1981) Hormone-sensitive lipase of rat adipose tissue. Purification and some properties. *J. Biol. Chem.* **256**, 6311–6320
 27. Ueno, M., Suzuki, J., Zenimaru, Y., Takahashi, S., Koizumi, T., Noriki, S., Yamaguchi, O., Otsu, K., Shen, W. J., Kraemer, F. B., and Miyamori, I. (2008) Cardiac overexpression of hormone-sensitive lipase inhibits myocardial steatosis and fibrosis in streptozotocin diabetic mice. *Am. J. Physiol. Endocrinol. Metab.* **294**, E1109–E1118
 28. Ueno, M., Suzuki, J., Hirose, M., Sato, S., Imagawa, M., Zenimaru, Y., Takahashi, S., Ikuyama, S., Koizumi, T., Konoshita, T., Kraemer, F. B., and Ishizuka, T. (2017) Cardiac overexpression of perilipin 2 induces dynamic steatosis: prevention by hormone-sensitive lipase. *Am. J. Physiol. Endocrinol. Metab.* **313**, E699–E709
 29. Sato, S., Suzuki, J., Hirose, M., Yamada, M., Zenimaru, Y., Nakaya, T., Ichikawa, M., Imagawa, M., Takahashi, S., Ikuyama, S., Konoshita, T., Kraemer, F. B., and Ishizuka, T. (2019) Cardiac overexpression of perilipin 2 induces atrial steatosis, connexin 43 remodeling, and atrial fibrillation in aged mice. *Am. J. Physiol. Endocrinol. Metab.* **317**, E1193–E1204
 30. Suzuki, J., Ueno, M., Uno, M., Hirose, Y., Zenimaru, Y., Takahashi, S., Osuga, J., Ishibashi, S., Takahashi, M., Hirose, M., Yamada, M., Kraemer, F. B., and Miyamori, I. (2009) Effects of hormone-sensitive lipase disruption on cardiac energy metabolism in response to fasting and refeeding. *Am. J. Physiol. Endocrinol. Metab.* **297**, E1115–E1124
 31. Kwong, S. C., Jamil, A. H. A., Rhodes, A., Taib, N. A., and Chung, I. (2019) Metabolic role of fatty acid binding protein 7 in mediating triple-negative breast cancer cell death via PPAR- α signaling. *J. Lipid Res.* **60**, 1807–1817
 32. Bligh, E. G., and Dyer, W. J. (1959) A rapid method of total lipid extraction and purification. *Can. J. Biochem. Physiol.* **37**, 911–917
 33. Schreiber, R., Hofer, P., Taschler, U., Voshol, P. J., Rechberger, G. N., Kotzbeck, P., Jaeger, D., Preiss-Landl, K., Lord, C. C., Brown, J. M., Haemmerle, G., Zimmermann, R., Vidal-Puig, A., and Zechner, R. (2015) Hypophagia and metabolic adaptations in mice with defective ATGL-mediated lipolysis cause resistance to HFD-induced obesity. *Proc. Natl. Acad. Sci. U. S. A.* **112**, 13850–13855
 34. Kintscher, U., Foryst-Ludwig, A., Haemmerle, G., and Zechner, R. (2020) The Role of Adipose Triglyceride Lipase and Cytosolic Lipolysis in Cardiac Function and Heart Failure. *Cell Rep. Med.* **1**, 100001
 35. Kolattukudy, P. E., and Niu, J. (2012) Inflammation, endoplasmic reticulum stress, autophagy, and the monocyte chemoattractant protein-1/CCR2 pathway. *Circ. Res.* **110**, 174–189
 36. Kong, P., Christia, P., and Frangogiannis, N. G. (2014) The pathogenesis of cardiac fibrosis. *Cell Mol. Life Sci.* **71**, 549–574
 37. Shen, W. J., Sridhar, K., Bernlohr, D. A., and Kraemer, F. B. (1999) Interaction of rat hormone-sensitive lipase with adipocyte lipid-binding protein. *Proc. Natl. Acad. Sci. U. S. A.* **96**, 5528–5532
 38. Jenkins-Kruchten, A. E., Bennaars-Eiden, A., Ross, J. R., Shen, W. J., Kraemer, F. B., and Bernlohr, D. A. (2003) Fatty acid-binding protein-hormone-sensitive lipase interaction. Fatty acid dependence on binding. *J. Biol. Chem.* **278**, 47636–47643
 39. Brejchova, K., Radner, F. P. W., Balas, L., Paluchova, V., Cajka, T., Chodounska, H., Kudova, E., Schratler, M., Schreiber, R., Durand, T., Zechner, R., and Kuda, O. (2021) Distinct roles of adipose triglyceride lipase and hormone-sensitive lipase in the catabolism of triacylglycerol estolides. *Proc. Natl. Acad. Sci. U. S. A.* **118**, e2020999118
 40. Ström, K., Gundersen, T. E., Hansson, O., Lucas, S., Fernandez, C., Blomhoff, R., and Holm, C. (2009) Hormone-sensitive lipase (HSL) is also a retinyl ester hydrolase: evidence from mice lacking HSL. *FASEB J.* **23**, 2307–2316
 41. Kanehara, H., Suzuki, J., Zenimaru, Y., Takahashi, S., Oida, K., Shen, W. J., Kraemer, F. B., and Miyamori, I. (2004) Function of hormone-sensitive lipase in diacylglycerol-protein kinase C pathway. *Diabetes Res. Clin. Pract.* **65**, 209–215

42. Sztalryd, C., and Kimmel, A. R. (2014) Perilipins: lipid droplet coat proteins adapted for tissue-specific energy storage and utilization, and lipid cytoprotection. *Biochimie*. **96**, 96–101
43. Wang, H., Hu, L., Dalen, K., Dorward, H., Marcinkiewicz, A., Russell, D., Gong, D., Londos, C., Yamaguchi, T., Holm, C., Rizzo, M. A., Brasaemle, D., and Sztalryd, C. (2009) Activation of hormone-sensitive lipase requires two steps, protein phosphorylation and binding to the PAT-1 domain of lipid droplet coat proteins. *J. Biol. Chem.* **284**, 32116–32125
44. Bickel, P. E., Tansey, J. T., and Welte, M. A. (2009) PAT proteins, an ancient family of lipid droplet proteins that regulate cellular lipid stores. *Biochim. Biophys. Acta*. **1791**, 419–440
45. Schweiger, M., Eichmann, T. O., Taschler, U., Zimmermann, R., Zechner, R., and Lass, A. (2014) Measurement of lipolysis. *Methods Enzymol.* **538**, 171–193
46. Kirschner, J., and Cathomen, T. (2020) Gene Therapy for Monogenic Inherited Disorders. *Dtsch. Arztebl. Int.* **117**, 878–885
47. High, K. A., and Roncarolo, M. G. (2019) Gene Therapy. *N. Engl. J. Med.* **381**, 455–464
48. Gaudet, D., Méthot, J., Déry, S., Brisson, D., Essiembre, C., Tremblay, G., Tremblay, K., de Wal, J., Twisk, J., van den Bulk, N., Sier-Ferreira, V., and van Deventer, S. (2013) Efficacy and long-term safety of alipogene tiparvovec (AAV1-LPLS447X) gene therapy for lipoprotein lipase deficiency: an open-label trial. *Gene Ther.* **20**, 361–369
49. Ong, T., Pennesi, M. E., Birch, D. G., Lam, B. L., and Tsang, S. H. (2019) Adeno-associated viral gene therapy for inherited retinal disease. *Pharm. Res.* **36**, 34
50. Al-Zaidy, S. A., and Mendell, J. R. (2019) From clinical trials to clinical practice: practical considerations for gene replacement therapy in SMA type I. *Pediatr. Neurol.* **100**, 3–11
51. Chen, S. J., Rader, D. J., Tazelaar, J., Kawashiri, M., Gao, G., and Wilson, J. M. (2000) Prolonged correction of hyperlipidemia in mice with familial hypercholesterolemia using an adeno-associated viral vector expressing very-low-density lipoprotein receptor. *Mol. Ther.* **2**, 256–261
52. Reid, B. N., Ables, G. P., Otlivanchik, O. A., Schoiswohl, G., Zechner, R., Blaner, W. S., Goldberg, I. J., Schwabe, R. F., Chua, S. C., Jr., and Huang, L. S. (2008) Hepatic overexpression of hormone-sensitive lipase and adipose triglyceride lipase promotes fatty acid oxidation, stimulates direct release of free fatty acids, and ameliorates steatosis. *J. Biol. Chem.* **283**, 13087–13099
53. Fortier, M., Soni, K., Laurin, N., Wang, S. P., Mauriège, P., Jirik, F. R., and Mitchell, G. A. (2005) Human hormone-sensitive lipase (HSL): expression in white fat corrects the white adipose phenotype of HSL-deficient mice. *J. Lipid Res.* **46**, 1860–1867